Transport properties of stage-1 $Cu_cCo_{1-c}Cl_2$ graphite intercalation compounds

1996 J. Phys.: Condens. Matter 8 7277

(http://iopscience.iop.org/0953-8984/8/39/006)

J. Phys.: Condens. Matter **8** (1996) 7277–7301. Printed in the UK

Transport properties of stage-1 $Cu_cCo_{1-c}Cl_2$ graphite intercalation compounds

Itsuko S Suzuki, Takehiko Shima, Brian Olson† and Masatsugu Suzuki

Department of Physics, State University of New York at Binghamton, Binghamton, NY 13902-6016, USA

Received 17 April 1996, in final form 17 June 1996

Abstract. Stage-1 $Cu_cCo_{1-c}Cl_2$ graphite intercalation compounds approximate quasi-two-dimensional (2D) random spin systems with competing ferromagnetic and antiferromagnetic intraplanar exchange interactions. The temperature dependence of the in-plane electrical resistivity of these compounds has been measured near critical temperatures. The magnetic resistivity ζ_{mag} consists of the long-range spin-order part ζ_{LS} and the spin-fluctuation part ζ_{SF}. For $0 \leqslant c \leqslant 0.2$ the long-range spin-order part ζ_{LS} is dominant: the temperature dependence of ζ_{LS} is described by a smeared power law with an exponent 2β, where β is the critical exponent of staggered magnetization. For $0.3 \leqslant c \leqslant 0.4$ the spin-fluctuation part ζ_{SF} becomes larger than ζ_{LS}. For $0.5 \leqslant c \leqslant 0.95$ no appreciable magnetic resistivity is observed. For $c = 1$ the derivative $-\mathrm{d}\zeta_{mag}/\mathrm{d}T$ shows a small peak at around 67 K due to the growth of short-range spin order which is characteristic of the 2D Heisenberg antiferromagnet. The critical behaviour of the in-plane resistivity can be explained in terms of a model based on $\pi-\mathrm{d}$ exchange interactions between π-electrons in the graphite layers and magnetic spins in the intercalate layers. The π-electrons are scattered by spins of a virtual antiferromagnetic in-plane spin configuration arising from the superposition of two ferromagnetic in-plane structures with spin directions antiparallel to each other. The $\pi-\mathrm{d}$ exchange interactions of these compounds are also discussed.

1. Introduction

Recently transport properties of magnetic graphite intercalation compounds (GICs) near a critical temperature T_c for the magnetic phase transition have aroused considerable interest [1–9]. In these compounds π-electrons in the graphite layers interact with magnetic spins in the intercalate layers through $\pi-\mathrm{d}$ exchange interactions. Consequently the electrical conduction of π-electrons in the graphite layers is influenced by both the long-range spin order appearing below T_c and the short-range spin order starting to grow well above T_c in the intercalate layers. In a previous paper [9] we have reported that the in-plane electrical resistivity of stage-1 $Co_cM_{1-c}Cl_2$ GICs (M = Mn and Mg) with $c \approx 1$ drastically increases with decreasing temperature below T_c. In order to explain such an anomaly for stage-1 $CoCl_2$ GICs we have proposed a model (see section 2 for details) based on the $\pi-\mathrm{d}$ exchange interaction which is defined as [2]

$$H_{\pi-d} = -\sum_{\boldsymbol{R}} J_{\pi-d}(\boldsymbol{r}-\boldsymbol{R})\boldsymbol{\sigma}_{\boldsymbol{r}} \cdot \boldsymbol{S}_{\boldsymbol{R}} \tag{1}$$

where $\boldsymbol{S}_{\boldsymbol{R}}$ is the spin vector of Co^{2+} at the position $\boldsymbol{R}$ in the intercalate layer and $\boldsymbol{\sigma}_{\boldsymbol{r}}$ is the spin vector of the π-electron at $\boldsymbol{r}$ in the graphite layer. In this compound the two-dimensional (2D) ferromagnetic layers are antiferromagnetically stacked along the c-axis

† Present address: Department of Physics, Case Western Reserve University, Cleveland, OH 44106, USA

0953-8984/96/397277+25$19.50

below T_c: these adjacent intercalate layers are structurally correlated. The π-electrons in the graphite layer are coupled with Co^{2+} spins in the two nearest-neighbour (N.N.) intercalate layers through the $\pi-$d exchange interactions. The π-electrons can be treated as if they are scattered by antiferromagnetically ordered Co^{2+} spins in one intercalate layer (2D antiferromagnet) located at a distance from the graphite layer. The magnetic resistivity near T_c is predicted to be described as a sum of the resistivity due to the staggered magnetization and that due to the staggered susceptibility or antiferromagnetic spin fluctuation. The drastic increase of the in-plane resistivity below T_c for stage-1 $Co_cM_{1-c}Cl_2$ GICs with $c \approx 1$ mainly comes from the temperature dependence of the staggered magnetization. The resistivity due to spin fluctuations is much smaller than that due to the staggered magnetization.

In this paper we report experimental results on the temperature dependence of the in-plane electrical resistivity for stage-1 $Cu_cCo_{1-c}Cl_2$ GICs in the temperature range between 4.6 and 300 K. In these compounds Cu^{2+} and Co^{2+} spins are randomly distributed on a triangular lattice in the $Cu_cCo_{1-c}Cl_2$ layers. In spite of relatively short c-axis repeat distance for stage-1 compounds, the interplanar exchange interaction is much weaker than the intraplanar exchange interaction. The ferromagnetic intraplanar exchange interaction between Co^{2+} spins competes with the antiferromagnetic intraplanar exchange interaction between Cu^{2+} spins. The growth of the in-plane spin-correlation length near T_c is limited by a spin-frustration effect arising from this competition. This spin-frustration effect is enhanced as the Cu concentration increases, suggesting that the resistivity due to spin fluctuations becomes dominant compared with that due to long-range spin order. The temperature dependence of the in-plane resistivity near T_c is discussed in terms of our model.

In section 2 we present a brief review on the magnetic properties of stage-2 $Cu_cCo_{1-c}Cl_2$ GICs [10, 11]. We also give a brief review on our model for the in-plane resistivity of stage-1 $CoCl_2$ GICs near T_c. In section 3 we discuss the experimental procedure. In section 4 we report the experimental results on $(00L)$ x-ray scattering, in-plane resistivity, and ac magnetic susceptibility for stage-1 $Cu_cCo_{1-c}Cl_2$ GICs. In section 5 the temperature dependence of the in-plane resistivity near T_c is discussed in the light of our model.

2. Background

2.1. Magnetic properties of stage-2 $Cu_cCo_{1-c}Cl_2$ GICs [10, 11]

The magnetic properties of stage-2 $Cu_cCo_{1-c}Cl_2$ GICs are considered to be almost the same as those of stage-1 $Cu_cCo_{1-c}Cl_2$ GICs. Here we show the magnetic properties of stage-2 $Cu_cCo_{1-c}Cl_2$ GICs which have been studied in detail [11]. The stage-2 $CoCl_2$ GIC magnetically behaves like a two-dimensional (2D) Heisenberg ferromagnet (fictitious spin $S = 1/2$) with large XY anisotropy. The Co^{2+} ions form a triangular lattice with side $a = 3.55$ Å. The spin Hamiltonian for Co^{2+} ions is described by the intraplanar exchange interaction ($J = 7.75$ K), the anisotropic exchange interaction J_A ($J_A/J = 0.48$) showing XY anisotropy, and the antiferromagnetic interplanar exchange interaction J'. The antiferromagnetic interplanar exchange interaction is very weak compared to the intraplanar exchange interaction: $|J'|/J = 8 \times 10^{-4}$. This compound shows two magnetic phase transitions at $T_{cu} = 9.1$ K and $T_{cl} = 8.0$ K. Above T_{cu} the system is in the paramagnetic phase. In the intermediate phase between T_{cl} and T_{cu} the system has 2D spin ordering. There is no spin correlation between adjacent $CoCl_2$ layers. Below T_{cl} the 3D antiferromagnetic phase occurs: the 2D ferromagnetic layers are antiferromagnetically stacked along the c-axis. The stage-2 $CuCl_2$ GIC magnetically behaves like a 2D Heisenberg antiferromagnet

on an isosceles triangular lattice with one short side ($a = 3.30$ Å) and two longer sides ($b = 3.72$ Å). The average exchange interaction between Cu^{2+} spins is antiferromagnetic and is given by $\langle J \rangle = -34$ K. No magnetic phase transition is observed either by dc magnetic susceptibility down to 1.5 K or by magnetic neutron scattering down to 0.3 K, due to the spin-frustration effect arising from the fully frustrated nature of the antiferromagnet on the triangular lattice.

Stage-2 $Cu_cCo_{1-c}Cl_2$ GICs provide a model system for studying the phase transition of spin-frustrated systems having competing ferromagnetic and antiferromagnetic interactions. The Cu^{2+} ion is a magnetic Jahn–Teller ion and the Co^{2+} ion is a magnetic non-Jahn–Teller ion. These ions are randomly distributed over the same intercalate layer. The intraplanar exchange interaction between Cu^{2+} spins is antiferromagnetic, while the intraplanar exchange interaction between Co^{2+} spins is ferromagnetic. The sign of the Curie–Weiss temperature changes from positive to negative with increasing Cu concentration at around $c = 0.80$ to 0.85. The intraplanar exchange interaction J(Cu–Co) between Cu^{2+} and Co^{2+} spins is ferromagnetic and increases with increasing Cu concentration. Those systems with $c < 0.9$ undergo a ferromagnetic phase transition at the critical temperature T_c. The irreversible effect of magnetization is observed below T_c: the zero-field-cooled (ZFC) magnetization deviates downward from the field-cooled (FC) magnetization below T_c and shows a broad peak at a temperature T_{max}. The low-temperature phase below T_c may correspond to a cluster glass phase where the spin direction of ferromagnetic clusters is frozen because of frustrated inter-island interactions which include a dipole–dipole interaction and an interplanar antiferromagnetic interaction. The critical temperature T_c increases as c increases and exhibits a broad maximum at around $c = 0.5$. This enhancement of T_c is partly due to the ferromagnetic interaction J(Cu–Co). No magnetic phase transition is observed for $0.9 < c < 1$ because of the spin-frustration effects arising from (i) the competition between ferromagnetic J(Cu–Co) and antiferromagnetic J(Cu–Cu) interactions, and (ii) the fully frustrated nature of the antiferromagnet on the triangular lattice.

2.2. The model for in-plane resistivity of the stage-1 $CoCl_2$ GIC [9]

We present a brief review of our model for the in-plane resistivity in the stage-1 $CoCl_2$ GIC due to the long-range spin order and spin fluctuation. Structurally the $CoCl_2$ layers stack in an ordered $\alpha\beta\gamma\alpha\beta\gamma$ rhombohedral sequence. The translation of the α-$CoCl_2$ layer by the vectors $\boldsymbol{\delta}$ $(=(2\boldsymbol{a} + \boldsymbol{b})/3)$ and $-\boldsymbol{\delta}$ gives rise to β- and γ-$CoCl_2$ layers, respectively, where $\boldsymbol{a}$ and $\boldsymbol{b}$ are the primitive lattice vectors: $|\boldsymbol{a}| = |\boldsymbol{b}| = 3.55$ Å and the angle between $\boldsymbol{a}$ and $\boldsymbol{b}$ is 120°. The Co^{2+} spins in each $CoCl_2$ layer become ferromagnetically ordered at low temperatures. Below T_c these 2D ferromagnetic layers are antiferromagnetically stacked along the c-axis [12, 13]. The π-electrons in the graphite layers are magnetically coupled with Co^{2+} spins of the $CoCl_2$ layers through the $\pi-$d exchange interaction. The electrical conduction of π-electrons is influenced by the existence of long-range in-plane spin orders of $CoCl_2$ layers. The π-electrons experience two kinds of molecular field which are antiparallel to each other. These molecular fields arise from the Co^{2+} spins of two structurally correlated $CoCl_2$ layers next to the graphite layer. For π-electrons the $\pi-$d interaction effect from Co^{2+} spins in one N.N. $CoCl_2$ layer is exactly the same as that in the other N.N. $CoCl_2$ layer, implying that the scattering of π-electrons by Co^{2+} spins is equivalent to that by Co^{2+} spins in the resultant antiferromagnetic in-plane spin configuration which is formed of the superposition of the in-plane ferromagnetic spin configurations of Co^{2+} in these two $CoCl_2$ layers. In other words, the π-electrons in the graphite layer can

be treated as if they are scattered by antiferromagnetically ordered Co^{2+} spins in one $CoCl_2$ layer (2D antiferromagnet), which is located at a distance 4.72 Å from the graphite layer.

The in-plane resistivity of the stage-1 $CoCl_2$ GIC is reduced to that for the 2D antiferromagnet. For the elastic scattering the magnetic resistivity of the system due to the $\pi-$d exchange interaction is described as

$$\rho_{mag} = \frac{\rho^0_{mag}}{\pi k_F^2} \int_0^{2k_F} \mathrm{d}Q \; f(Q)\Gamma(\boldsymbol{Q}) \tag{2}$$

where $\boldsymbol{Q}$ is the in-plane scattering wave vector, $\Gamma(\boldsymbol{Q})$ is the Fourier transform of the spin-correlation function, k_F is the Fermi wave number, ρ^0_{mag} is the electrical resistivity in the high-temperature limit, and the function $f(Q)$ is defined by

$$f(Q) = \frac{Q^2}{\sqrt{4k_F^2 - Q^2}}. \tag{3}$$

The function $f(Q)$ is equal to zero at $Q = 0$ and monotonically increases with increasing Q. The spin-correlation function $\Gamma(\boldsymbol{Q})$ near $\boldsymbol{Q} = \boldsymbol{Q}_0$ can be described by

$$\Gamma(\boldsymbol{Q}) = \chi(\boldsymbol{Q}) = \frac{\chi(\boldsymbol{Q}_0)}{1 + |\boldsymbol{Q} - \boldsymbol{Q}_0|^2/\kappa^2} \tag{4}$$

where $\boldsymbol{Q}_0$ is the in-plane wave vector for the antiferromagnetic Bragg point, κ is the spin-correlation length, $\chi(\boldsymbol{Q} = \boldsymbol{Q}_0) = \chi_s T$ and the staggered susceptibility χ_s diverges at T_c: $\chi_s \approx \kappa^{-2+\eta}$. Note that ν and η are the critical exponent of spin-correlation length and the Fisher–Burford critical exponent, respectively, for $T > T_c$. Then the resistivity ρ_{mag} is predicted as $\rho_{mag} \approx \kappa\chi(\boldsymbol{Q} = \boldsymbol{Q}_0) \approx \kappa^{-1+\eta}$, or the form

$$\rho_{mag} = \rho_2 |t|^{\nu(-1+\eta)} \qquad (T > T_c) \tag{5}$$

where $t = (T - T_c)/T_c$ and ρ_2 is a constant with the dimension of resistivity. This form indicates that ρ_{mag} diverges at T_c on approaching T_c from above since η is a small positive value. On the other hand, the spin-correlation function $\Gamma(\boldsymbol{Q})$ below T_c is described as

$$\Gamma(\boldsymbol{Q}) = \langle S_{\boldsymbol{Q}=\boldsymbol{Q}_0}\rangle^2 \delta(\boldsymbol{Q} - \boldsymbol{Q}_0) + \frac{\chi(\boldsymbol{Q}_0)}{1 + |\boldsymbol{Q} - \boldsymbol{Q}_0|^2/\kappa^2} \tag{6}$$

where $\langle S_{\boldsymbol{Q}=\boldsymbol{Q}_0}\rangle$ is proportional to the staggered magnetization M_s of the system. The magnetization M_s varies with temperature as $|t|^\beta$, where β is the critical exponent of magnetization. Then ρ_{mag} is given by a sum of the contributions related to the staggered magnetization and staggered susceptibility, or the form

$$\rho_{mag} \approx \rho_1' |t|^{2\beta} + \rho_2' |t|^{\nu'(-1+\eta')} \qquad (T < T_c) \tag{7}$$

where ρ_1' and ρ_2' are constants with the dimension of resistivity, ν' and η' are the corresponding critical exponents for $T < T_c$. In the limit of $\rho_1' \gg \rho_2'$ the resistivity ρ_{mag} varies with temperature as $|t|^{2\beta}$. In the above discussion we neglect the effect arising from the fact that the spins separated by a distance greater than the electron mean free path cannot scatter π-electrons coherently. If this effect is appropriately included in the model, the divergence of the resistivity in (5) and (7) near T_c may be greatly suppressed [14, 15]. The model described above is expected to be applicable to the in-plane resistivity of stage-1 $Cu_cCo_{1-c}Cl_2$ GICs with low Cu concentration c.

3. Experimental procedure

Intercalants were prepared from reagent-grade $CuCl_2$ and $CoCl_2$ powders. These powders were dehydrated at 350 °C in the presence of HCl gas at one atmosphere. Single crystals of $Cu_cCo_{1-c}Cl_2$ over the entire range of Cu concentrations were grown by heating a mixture of dehydrated $CuCl_2$ and $CoCl_2$ with nominal weight composition at 780 °C in a quartz tube sealed in vacuum. $Cu_cCo_{1-c}Cl_2$ GIC samples with $c \geqslant 0.2$ were synthesized by intercalation of $Cu_cCo_{1-c}Cl_2$ into highly oriented pyrolytic graphite (HOPG): the mixture of HOPG and $Cu_cCo_{1-c}Cl_2$ was heated at 450 °C for 14 days in Pyrex glass sealed in vacuum. The stage-1 $CoCl_2$ GIC sample was synthesized by intercalation of $CoCl_2$ into single-crystal kish graphite (SCKG): the mixture of SCKG and $CoCl_2$ was heated at 520 °C for 20 days in the presence of chlorine gas at a pressure of 740 Torr.

Table 1. Fraction of stage 1 for $Cu_cCo_{1-c}Cl_2$ GIC samples with stoichiometry $C_nCu_cCo_{1-c}Cl_2$, where c is the nominal Cu concentration. The fraction of stage 1 can be estimated from (11) with the integrated intensity ratio of $(002)_1$ reflection for stage 1 to $(003)_2$ reflection for stage 2.

c	n	Ratio	Stage 1 (%)
0	5.76		≈100
0.20	8.08		≈100
0.30	6.39		
0.40	7.51	4.85	72
0.50	6.85	3.97	69
0.60	8.49	0.96	53
0.70	9.16	2.87	66
0.80	5.70	1.67	60
0.85	8.39		
0.90	8.40	2.02	62
0.98	7.11		
1	6.85		≈100

The staging structure of $Cu_cCo_{1-c}Cl_2$ GIC samples was determined from $(00L)$ x-ray scattering measurements made at 295 K using a Huber double-circle diffractometer with a Mo Kα x-ray radiation source (1.5 kW) and HOPG monochromator. An entrance slit of 2×2 mm^2 was placed between the monochromator and the sample. The x-ray beam diffracted by the sample was collimated using an exit slit of 1×1 mm^2 and detected with a Bicron photomultiplier tube.

The Cu concentration of the $Cu_cCo_{1-c}Cl_2$ GIC samples was determined from dc magnetic susceptibility and electron microprobe measurement. The dc magnetic susceptibility was measured using a Faraday balance method in the temperature range between 100 and 300 K. A quartz bucket containing the sample was suspended from a fine quartz fibre attached to a Cahn electrobalance. The dc magnetic susceptibility of $Cu_cCo_{1-c}Cl_2$ GICs obeys the Curie–Weiss law in the temperature range between 150 and 300 K [10]. The effective magnetic moment $P_{eff}(c)$ derived from the Curie–Weiss constant is predicted as

$$P_{eff}(c) = [cP_{eff}^2(\mathrm{Cu}^{2+}) + (1-c)P_{eff}^2(\mathrm{Co}^{2+})]^{1/2} \tag{8}$$

from a molecular-field theory, where $P_{eff}(\mathrm{Cu}^{2+})$ $(=2.33\mu_B)$ and $P_{eff}(\mathrm{Co}^{2+})$ $(=5.51\mu_B)$ are the effective magnetic moments of Cu^{2+} and Co^{2+} spins for the stage-1 $CuCl_2$ GIC [11] and $CoCl_2$ GIC [16], respectively. The macroscopic Cu concentration c for each

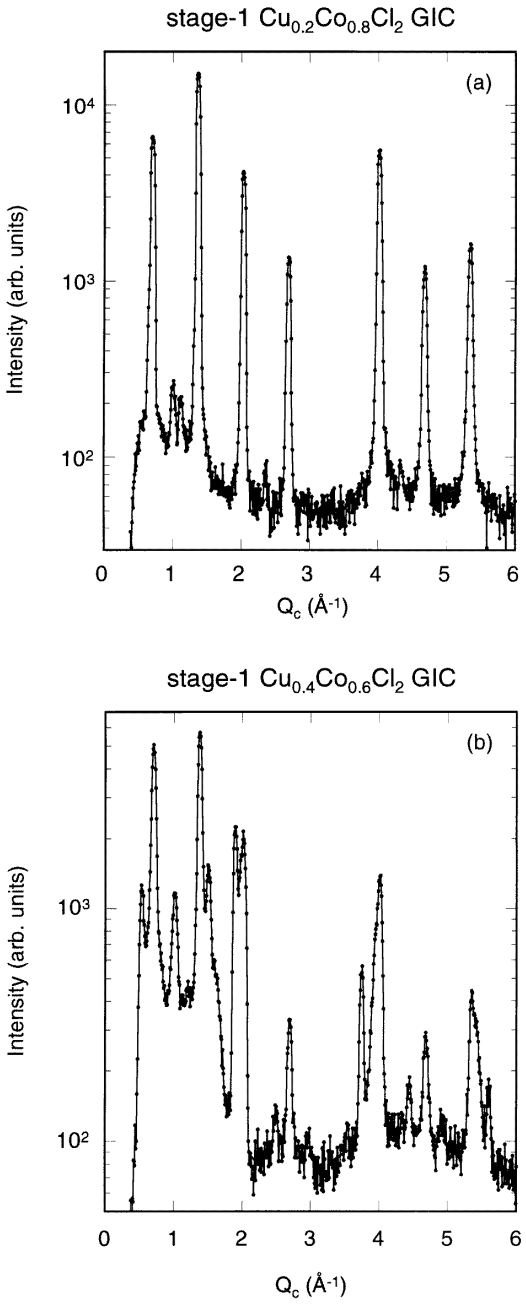

Figure 1. $(00L)$ x-ray diffraction patterns for $Cu_cCo_{1-c}Cl_2$ GIC samples with (a) $c = 0.20$ and (b) $c = 0.40$ at 295 K, where Q_c is the wave number along the c^*-axis. (c) $L^{(1)}$-dependence of the peak shift $\Delta_{PS}^{(1)}$ of the $(00L)_1$ Bragg reflection from $Q_c^{(1)} = (2\pi/d_1)L^{(1)}$ for samples with $c = 0.20$ (●), 0.40 (○), and 0.60 (▲), where $L^{(1)}$ is the Bragg index for stage 1. (d) $L^{(2)}$-dependence of $\Delta_{PS}^{(2)}$ of the $(00L)_2$ Bragg reflection from $Q_c^{(2)} = (2\pi/d_2)L^{(2)}$ for samples with $c = 0.40$ (○) and 0.60 (▲), where $L^{(2)}$ is the Bragg index for stage 2.

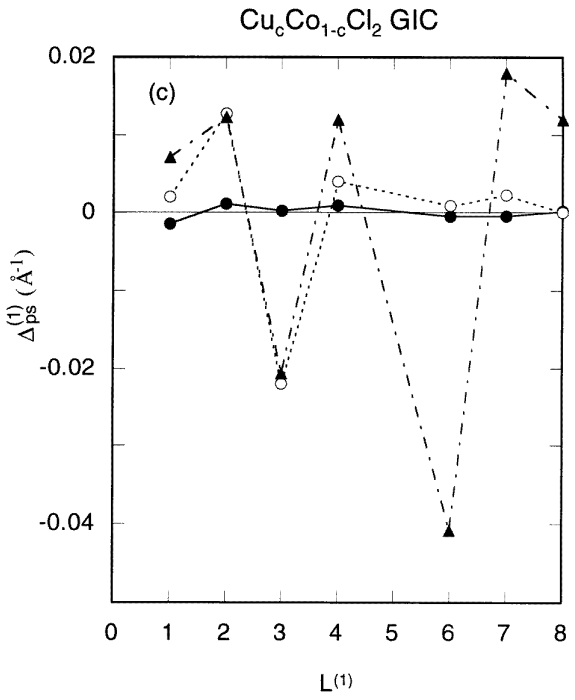

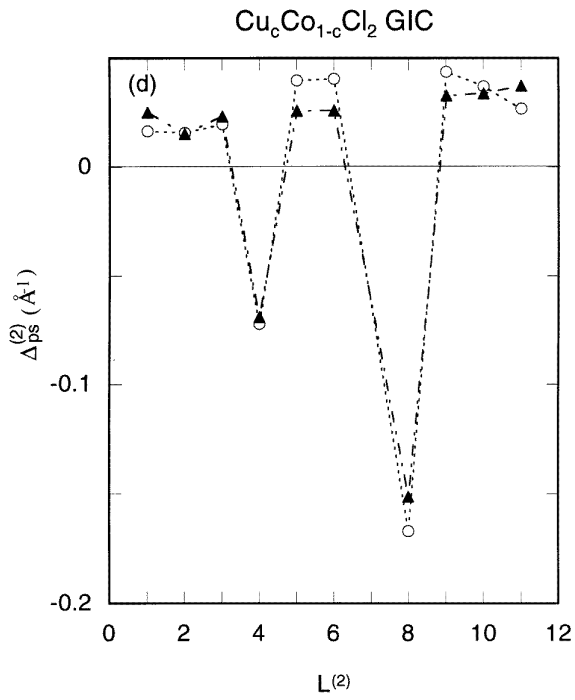

Figure 1. (Continued)

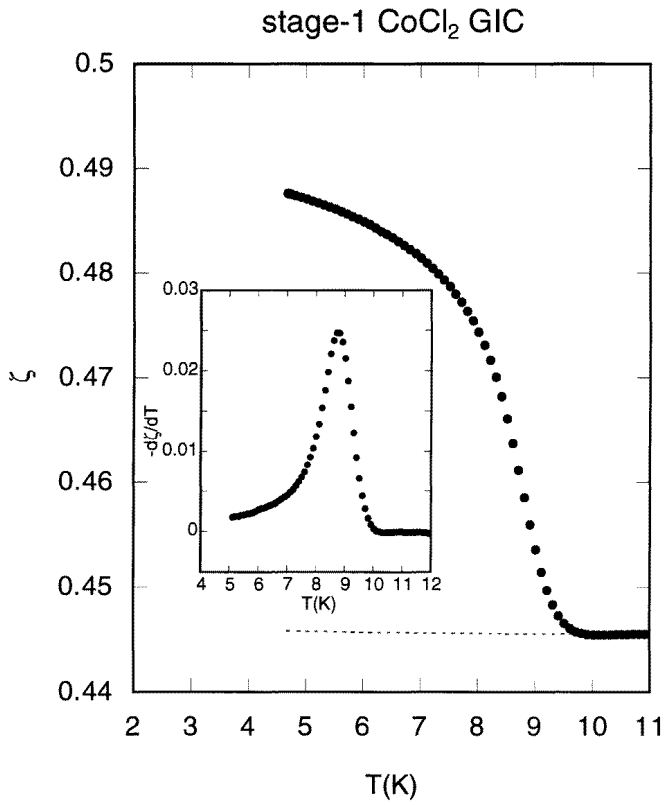

Figure 2. The temperature dependence of the normalized in-plane resistivity defined by $\zeta = \rho_a(T)/\rho_a(T = 290\ \mathrm{K})$ and $-\mathrm{d}\zeta/\mathrm{d}T$ (shown in the inset) for the stage-1 $CoCl_2$ GIC near T_c [9]. The dotted line is the extrapolation of $\zeta_{non-mag}$ from the high-temperature side.

sample estimated from (8) with the measured value of $P_{eff}(c)$ is in good agreement with a nominal Cu concentration of the $Cu_cCo_{1-c}Cl_2$ bulk sample. The electron microprobe measurement was carried out using a scanning electron microscope (Model Hitachi S-450). Electrons having a kinetic energy of 20 keV penetrated the sample to a depth of the order of 2 μm, and spread out to a similar distance. The quoted concentration is the averaged value of measurements over several different points in the sample. The Cu concentration thus determined is also in good agreement with nominal Cu concentration of the $Cu_cCo_{1-c}Cl_2$ bulk sample.

The stoichiometry ($C_nCu_cCo_{1-c}Cl_2$) of each sample was determined from weight uptake measurements. The values of n for each Cu concentration are listed in table 1. The values of n for $c = 0.20$, 0.40, 0.60, 0.70, 0.85, 0.90, and 0.98 deviate from the ideal value of n: $n \approx 4.1$ for stage 1. This deviation may arise for the following reasons: (i) the formation of small islands in intercalate layers, leading to an incomplete filling factor, (ii) the mixture of fractions with stage 1 and the higher stage number (see section 4), and (iii) the Hendricks–Teller stage disorder (see section 4).

The in-plane electrical resistivity of $Cu_cCo_{1-c}Cl_2$ GICs was measured in the temperature range between 4.6 and 300 K using a conventional four-probe method. The samples had a rectangular form with typically a 7 mm $\times$ 2 mm base and a height of 0.5 mm. Four thin

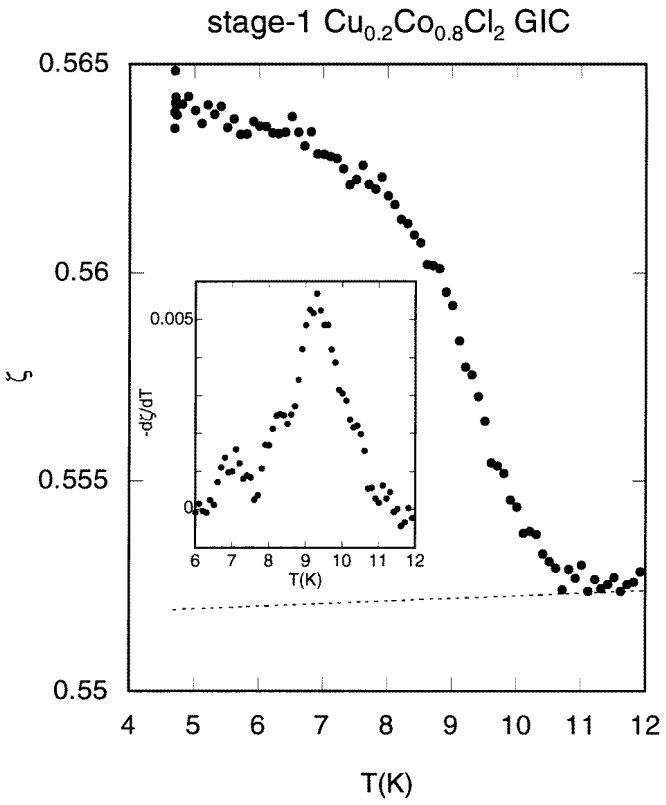

Figure 3. The temperature dependence of ζ and $-\mathrm{d}\zeta/\mathrm{d}T$ (shown in the inset) for the stage-1 $Cu_cCo_{1-c}Cl_2$ GIC with $c = 0.20$ near T_c. The dotted line is the extrapolation of $\zeta_{non-mag}$ from the high-temperature side.

gold wires (25 μm in diameter) as the current and voltage probes were attached to the base of the sample with silver paste (4922N, du Pont) which was diluted with 2-butoxyethyl acetate: voltage probes were located on a straight line between current probes. The sample was mounted on the copper surface of a heat sink which was electrically insulated by a varnish (GE-7031). The current (typically 1–50 mA) was supplied through the current probes by a programmable current source (Keithley, Model 224). The voltage generated across the voltage probes was measured by a digital nanovoltmeter (Keithley, Model 181). The temperatures of samples were measured with a silicon diode sensor (DT-470, SD13) embedded in the copper heat sink, which was supplied by a 10 μA current source. We note that the absolute value of the resistivity cannot be exactly determined by the four-probe method used here. The measured resistivity is very sensitive to the location of probes, the area of silver paste on the sample surface, the distance between voltage probes, the degree of roughness of sample surfaces, and so on. Hereafter we report only the normalized in-plane resistivity defined by $\zeta(T)$ $(=\rho_a(T)/\rho_a(290\ \mathrm{K}))$, which is independent of the above factors.

The critical temperatures of $Cu_cCo_{1-c}Cl_2$ GICs were determined from ac magnetic susceptibility measurement made by a conventional ac Hartshorn bridge method in the temperature range between 4.6 and 25 K. An ac magnetic field (0.3 Oe) of 330 Hz was applied in an arbitrary direction in the c-plane of the samples.

4. Results

4.1. Sample characterization: (00L) *x-ray scattering*

The c-axis stacking sequence of $Cu_cCo_{1-c}Cl_2$ GIC samples was determined from (00L) x-ray diffraction. Figures 1(a) and 1(b) show the (00L) x-ray scattering intensities for $Cu_cCo_{1-c}Cl_2$ GICs with $c = 0.20$ and $c = 0.40$ at 295 K, respectively. In figure 1(a) most peaks are indexed to stage-1 reflections $(00L)_1$ with a c-axis repeat distance of $d_1 = 9.481 \pm 0.002$ Å. In figure 1(b) strong peaks are indexed to stage-1 reflections $(00L)_1$ with $d_1 = 9.48 \pm 0.02$ Å and weak peaks are indexed to stage-2 reflections $(00L)_2$ with the c-axis repeat distance $d_2 = 12.93 \pm 0.03$ Å, indicating a mixture of majority stage 1 and minority stage 2. The ratio of the fraction with stage-1 structure to that with stage-2 structure can be estimated from the integrated intensities of stage-1 reflection $(002)_1$ and stage-2 reflection $(003)_2$. The (00L) x-ray intensities for systems with ideal stage-1 and stage-2 packages for $Cu_cCo_{1-c}Cl_2$ GICs are calculated as

$$\tilde{I}(00L)_1 = \{\rho_G f_G(Q_c^{(1)}) + (-1)^L[\rho_{Co} f_{Co}(Q_c^{(1)}) + \rho_{Cu} f_{Cu}(Q_c^{(1)}) + 2\rho_{Cl} f_{Cl}(Q_c^{(1)}) \cos(Q_c^{(1)} z_1)]\}^2 \tag{9}$$

and

$$\tilde{I}(00L)_2 = \{2\rho_G f_G(Q_c^{(2)}) \cos(Q_c^{(2)} c_1) + \rho_{Co} f_{Co}(Q_c^{(2)}) + \rho_{Cu} f_{Cu}(Q_c^{(2)}) + 2\rho_{Cl} f_{Cl}(Q_c^{(2)}) \cos(Q_c^{(2)} z_1)]\}^2 \tag{10}$$

respectively, where f_i is the atomic form factor depending on $Q_c^{(1)}$ and $Q_c^{(2)}$, ρ_i is the density of atom i, z_1 is the distance between the Cu_cCo_{1-c} layer and the Cl layer, $Q_c^{(1)} = 2\pi L/d_1$, $Q_c^{(2)} = 2\pi L/d_2$, L is the Bragg index, and c_1 the distance between the Cu_cCo_{1-c} layer and the graphite layer. Then the probabilities of finding stage-1 packages (p_1) and stage-2 packages (p_2) in a sample with a mixture of stage 1 and stage 2 are estimated from the relation

$$\frac{I(002)_1}{I(003)_2} = \frac{p_1^2}{p_2^2} \frac{\tilde{I}(002)_1}{\tilde{I}(003)_2} \tag{11}$$

with $p_1 + p_2 = 1$, where $I(002)_1$ and $I(003)_2$ are the integrated x-ray intensities for stage-1 reflection $(002)_1$ and for stage-2 $(003)_2$ reflection. Since the atomic form factor $f_{Co}(Q_c = 0)$ is almost the same as $f_{Cu}(Q_c = 0)$, the intensities $\tilde{I}(002)_1$ and $\tilde{I}(003)_2$ are assumed to be independent of Cu concentration. For convenience we use the ratio $\tilde{I}(002)_1/\tilde{I}(003)_2 = 0.775$ for the $CoCl_2$ GIC, where $\rho_G = 4.17$, $\rho_{Co} = \rho_{Cl} = 1$, $z_1 = 1.39$ Å, $c_1 = 4.72$ Å, $d_1 = 9.439$ Å, $d_2 = 12.789$ Å, $Q_c^{(1)} = 1.313$ Å^{-1} and $Q_c^{(2)} = 1.474$ Å^{-1}. The values of p_1 for each sample thus determined are listed in table 1.

Here we note that these values of p_1 and p_2 give only rough estimates for the fractions of stage-1 and stage-2 structures. For example, even well-defined (00L) Bragg reflections for stage 1 in figure 1(a) do not necessarily imply that $p_1 = 1$ because of the possibility for Hendricks–Teller stage disorder [17] with a random arrangement of packages with different stages along the c-axis. The effect of Hendricks–Teller stage disorder on the (00L) x-ray diffraction pattern for MCl_2 GIC (M = Co, Ni, Mn) has been theoretically discussed in a previous paper [18]. It is characterized by (i) the full width at half-maximum (FWHM) of Bragg reflections varying with the Bragg index L and (ii) the peak shift Δ_{PS} of Bragg reflections from that of the pure stage varying with the Bragg index L. Figure 1(c) shows the $L^{(1)}$-dependence of the peak shift $\Delta_{PS}^{(1)}$ of the stage-1 (00L) Bragg reflection from the average position $Q_c^{(1)} = (2\pi/d_1)L^{(1)}$ for samples with $c = 0.20$, 0.40, and 0.60, where $L^{(1)}$

is the stage-1 Bragg index. The peak shift $\Delta_{PS}^{(1)}$ for $c = 0.20$, 0.40, and 0.60 oscillates with the Bragg index $L^{(1)}$: a local maximum at $L^{(1)} = 2$ and local minima at $L^{(1)} = 3$ and 6. The amplitude of the oscillation in $\Delta_{PS}^{(1)}$ becomes large with increasing Cu concentration. When stage-1 and stage-2 packages with the probabilities of g_1 and g_2 ($g_1 \gg 0.5$ and $g_1 + g_2 = 1$) are randomly arranged along the c-axis, the Hendricks–Teller stage-disorder-induced peak shift $\Delta_{PS}^{(1)}$ for the $CoCl_2$ GIC is predicted by [18]

$$\Delta_{PS}^{(1)} = -\frac{g_2}{g_1 d_1} \sin(Q_c^{(1)} c_2) \tag{12}$$

where c_2 (= 3.35 Å) is the separation distance between graphite layers with no intervening $CoCl_2$ layer. The peak shift $\Delta_{PS}^{(1)}$ sinusoidally varies with the Bragg index $L^{(1)}$. For $d_1 = 9.439$ Å for the stage-1 $CoCl_2$ GIC the peak shift has local minima at $L^{(1)} = 2$, 5 and 8, and local maxima at $L^{(1)} = 1$, 3–4, and 6, which indicates that the observed variation of $\Delta_{PS}^{(1)}$ with $L^{(1)}$ in figure 1(c) is due to the Hendricks–Teller stage disorder with the random arrangements of majority stage-1 and minority stage-2 packages along the c-axis. According to (12) the amplitude of the oscillation in $\Delta_{PS}^{(1)}$ is proportional to the ratio g_2/g_1. From the value of $\Delta_{PS}^{(1)}$ at $L^{(1)} = 2$ the ratio g_2/g_1 can be estimated as 0.01 for $c = 0.20$, 0.13 for $c = 0.40$, and 0.12 for $c = 0.60$, indicating that the degree of stage disorder becomes higher as the Cu concentration increases.

Figure 1(d) shows the L-dependence of the peak shift $\Delta_{PS}^{(2)}$ of the stage-2 $(00L)$ Bragg reflection from the average position $Q_c^{(2)} = (2\pi/d_2)L^{(2)}$ for samples with $c = 0.40$ and $c = 0.60$, where $L^{(2)}$ is the Bragg index for stage 2. The peak shifts $\Delta_{PS}^{(2)}$ for $c = 0.40$ and $c = 0.60$ change with the Bragg index $L^{(2)}$: a local maximum at $L^{(2)} \approx$ 5–6 and local minima at $L^{(2)} = 4$ and 8. When stage-1, stage-2 and stage-3 packages with the probabilities g_1, g_2 and g_3 ($g_2 \gg 0.5$ and $g_1 + g_2 + g_3 = 1$) are randomly arranged along the c-axis, the peak shift $\Delta_{PS}^{(2)}$ is predicted by [18]

$$\Delta_{PS}^{(2)} = \frac{g_1 - g_3}{g_2 d_2} \sin(Q_c^{(2)} c_2) \tag{13}$$

which also sinusoidally varies with the Bragg index $L^{(2)}$. For $d_2 = 12.789$ Å for the $CoCl_2$ GIC the peak shift has local maxima at $L^{(2)} = 1$, 5, and 8–9, and local minima at $L^{(2)} = 3$ and 7 for $g_1 > g_3$, and local maxima at $L^{(2)} = 3$ and 7 and local minima at $L^{(2)} = 1$, 5, and 8–9 for $g_1 < g_3$. The comparison between the experimental results shown in figure 1(d) and the above prediction indicates that $g_1 < g_3$ for both $c = 0.40$ and $c = 0.60$.

In summary, we find that both mixture of stages and Hendricks–Teller stage disorder occur in $Cu_cCo_{1-c}Cl_2$ GIC samples. The stage-1 fraction is relatively larger than stage-2 and stage-3 fractions. Hereafter, for convenience, the samples used in the present experiment are denoted by stage-1 $Cu_cCo_{1-c}Cl_2$ GICs.

4.2. Magnetic resistivity

The temperature dependence of the in-plane resistivity $\rho_a(T)$ of stage-1 $Cu_cCo_{1-c}Cl_2$ GICs with $c = 0$, 0.20, 0.30, 0.40, 0.50, 0.60 0.70, 0.80, 0.90, 0.98, and 1 has been measured near critical temperatures. In figure 2 we show the temperature dependence of the normalized in-plane resistivity $\zeta(T)$ for $c = 0$ near T_c, which has been reported in the previous paper [9]. The in-plane resistivity $\zeta(T)$ exhibits a drastic increase below ≈10 K with decreasing temperature and almost saturates near 5 K. The degree of this drastic increase in ζ can be estimated from a relative value defined by

$$\Delta\tilde{\zeta} = \left(\frac{\zeta_{sat}}{\zeta_{min}} - 1\right) \times 100 \ (\%) \tag{14}$$

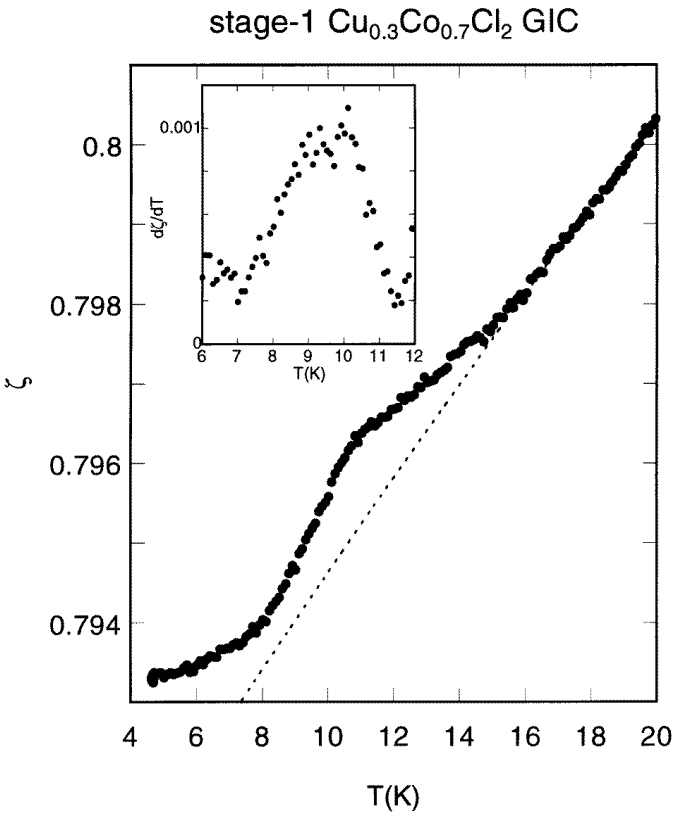

Figure 4. The temperature dependences of ζ and $\mathrm{d}\zeta/\mathrm{d}T$ (shown in the inset) for the stage-1 $Cu_cCo_{1-c}Cl_2$ GIC with $c = 0.30$ near T_c. The dotted line is the extrapolation of $\zeta_{non-mag}$ from the high-temperature side.

where ζ_{sat} and ζ_{min} are the saturated value of ζ at the lowest temperature and the minimum value of ζ, respectively. We find that our result for $\Delta\tilde{\zeta}$ (=9.7%) for $c = 0$ agrees well with that reported by Yeh *et al* [1] (10%). In the inset of figure 2 we show the temperature dependence of $-\mathrm{d}\zeta/\mathrm{d}T$ for $c = 0$, which exhibits a sharp peak with a peak value of 0.025 K^{-1} at around 8.73 K. This peak temperature is assumed to coincide with the critical temperature T_c, below which the 2D ferromagnetic $CoCl_2$ layers are antiferromagnetically stacked along the c-axis. Figure 3 shows the temperature dependence of ζ for $c = 0.20$ for $4.6 \leqslant T \leqslant 12$ K. Like the temperature dependence of ζ for $c = 0$, ζ for $c = 0.20$ also shows a drastic increase with decreasing temperature below $\approx$10.5 K and saturates near 5 K. The relative value $\Delta\tilde{\zeta}$ for $c = 0.20$ is estimated as 2.2%, indicating that $\Delta\tilde{\zeta}$ rapidly decreases with increasing Cu concentration. In the inset of figure 3 we show the temperature dependence of $-\mathrm{d}\zeta/\mathrm{d}T$ for $c = 0.20$, which has a relatively broad peak with a peak value of 0.0056 K^{-1} at $T_c = 9.30$ K.

Figure 4 shows the temperature dependence of ζ for $c = 0.30$ for $4.6 \leqslant T \leqslant 20$ K. Clearly it is very different from that for $c = 0$ and 0.20: the in-plane resistivity ζ for $c = 0.30$ increases with increasing temperature, showing a step-like increase in the temperature range between 8 and 11 K. In the inset of figure 4 we show the temperature dependence of $\mathrm{d}\zeta/\mathrm{d}T$ for $c = 0.30$, which has a positive sign for $4.6 \leqslant T \leqslant 300$ K and exhibits a very broad

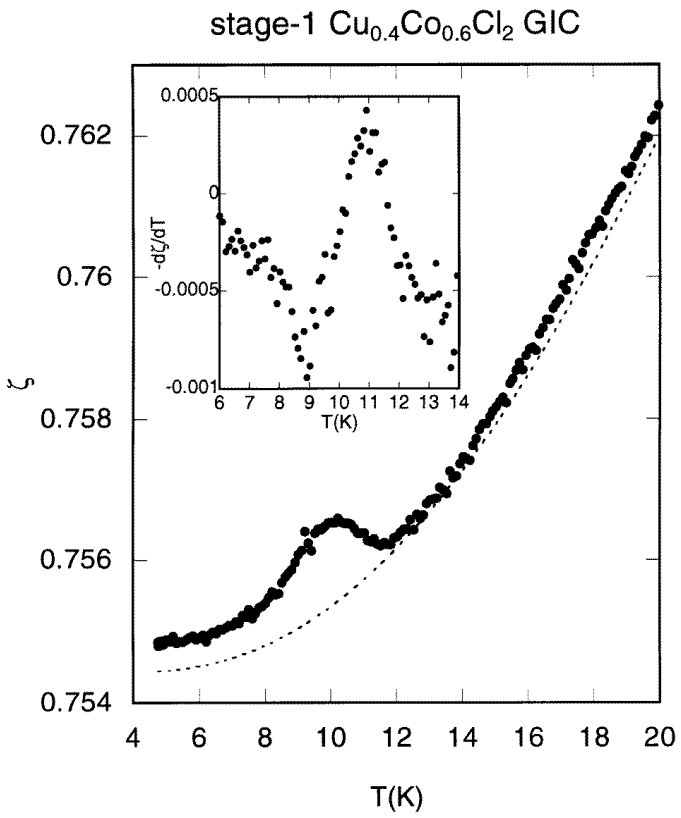

Figure 5. The temperature dependences of ζ and $-\mathrm{d}\zeta/\mathrm{d}T$ (shown in the inset) for the stage-1 $Cu_cCo_{1-c}Cl_2$ GIC with $c = 0.40$ near T_c. The dotted line is the extrapolation of $\zeta_{non-mag}$ from the high-temperature side.

peak with a peak value of 0.001 K^{-1} near $T_c = 9.43 \pm 0.02$ K. The peak value of $|\mathrm{d}\zeta/\mathrm{d}T|$ for $c = 0.30$ is much smaller than that for $c = 0$ and $c = 0.20$.

Figure 5 shows the temperature dependence of ζ for $c = 0.40$. The resistivity ζ has a small broad peak centred at 10.2 K. Except for this peak, ζ monotonically increases with increasing temperature. In the inset of figure 5 we show the temperature dependence of $-\mathrm{d}\zeta/\mathrm{d}T$ for $c = 0.40$, which is very different from those for $c = 0$, 0.20, and 0.30. It has a negative local minimum of -0.001 K^{-1} at 8.9 K and a positive local maximum of 0.0005 K^{-1} at 10.9 K. Here we assume that T_c ($=10.20 \pm 0.01$ K) is a temperature at which $-\mathrm{d}\zeta/\mathrm{d}T = 0$ or ζ has a peak.

Figure 6 shows the plots of ζ versus T for $4.6 \leqslant T \leqslant 20$ K: $c = 0.50$ and 0.60. Note that the data on ζ versus T for $c = 0.70$, 0.80, and 0.90 not shown here are very similar to those for $c = 0.50$ and $c = 0.60$. The resistivity ζ for $0.50 \leqslant c \leqslant 0.90$ monotonically increases with increasing temperature for $4.6 \leqslant T \leqslant 300$ K. No magnetic resistivity anomaly is observed in spite of the fact that the magnetic phase transition occurs between 8 and 11 K for systems with $c \leqslant 0.90$.

Figure 7 shows the temperature dependence of ζ for $c = 1$ for $4.6 \leqslant T \leqslant 90$ K, which has an appreciable step-like anomaly at around 67 K. In the inset of figure 7 we show the temperature dependence of $-\mathrm{d}\zeta/\mathrm{d}T$ for $c = 1$, which has a relatively broad peak at around

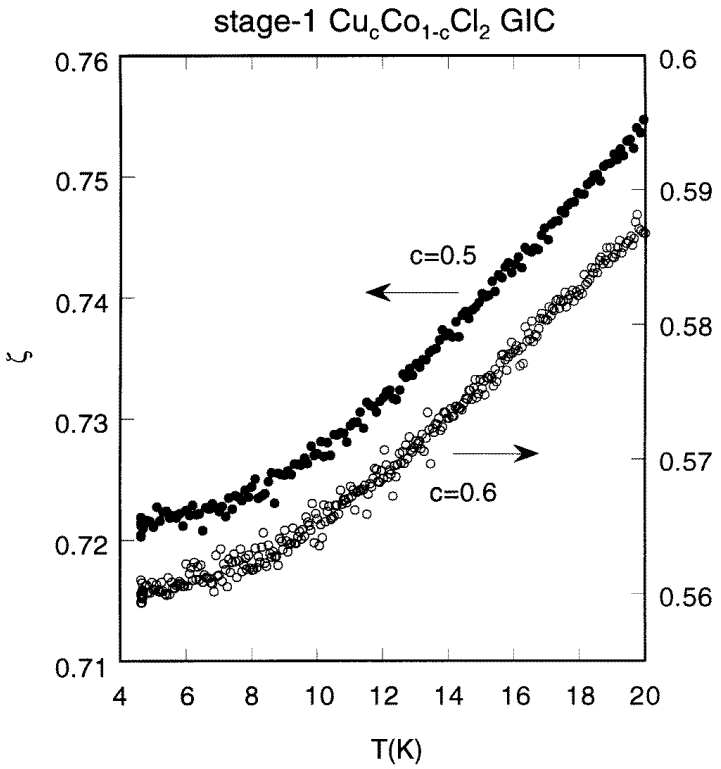

Figure 6. ζ versus T for stage-1 $Cu_cCo_{1-c}Cl_2$ GICs with $c = 0.50$ (●) and 0.60 (○) for $4.6 \leqslant T \leqslant 20$ K.

67 K. Here we note that the dc magnetic susceptibility of the stage-1 $CuCl_2$ GIC exhibits a broad peak of magnitude χ_{max} (=2.858×10^{-3} emu/Cu mol) at the temperature T_{max} (=65 K) [11]. The position and magnitude of this susceptibility maximum are consistent with those of a 2D Heisenberg antiferromagnet with the average antiferromagnetic intraplanar exchange interaction $\langle J \rangle$ (= − 39 K) [19]. Apart from this broad peak there is no anomaly in the dc magnetic susceptibility above 1.5 K. Therefore we can conclude that the resistivity anomaly near 67 K for $c = 1$ is due to the growth of antiferromagnetic short-range spin order developed in the $CuCl_2$ intercalate layers. This result also gives direct evidence for the exchange interaction between π-electrons and Cu^{2+} spins mediated through the p-orbital electrons of the Cl^- ions.

4.3. Non-magnetic resistivity

Figure 8 shows typical examples of ζ versus T for $2.6 \leqslant T \leqslant 290$ K: $c = 0.20$ and 1. We find that the resistivity ζ for $0 \leqslant c \leqslant 1$ monotonically increases with increasing temperature for $20 \leqslant T \leqslant 290$ K. The data on ζ versus T for these compounds fit well to the form

$$\zeta(T) = A_n + B_nT + C_nT^2 \tag{15}$$

with the coefficients A_n, B_n, and C_n. Here the characteristic temperature T_0 is defined as $T_0 = B_n/C_n$. The second term (B_nT) in (15) is due to the intrapocket electron–phonon scattering, while the third term (C_nT^2) is due to the interpocket electron–phonon scattering

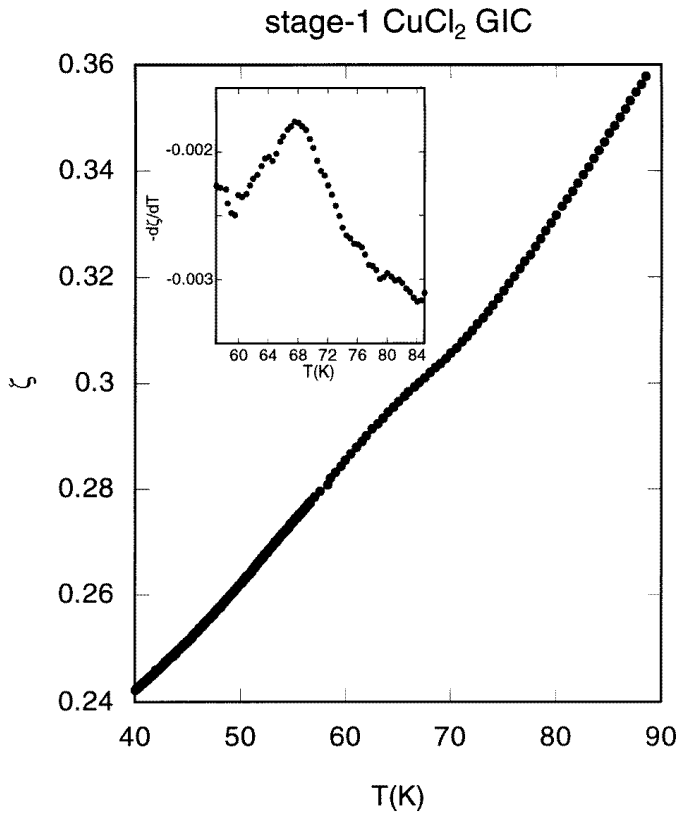

Figure 7. The temperature dependences of ζ and $-\mathrm{d}\zeta/\mathrm{d}T$ (shown in the inset) for the stage-1 $CuCl_2$ GIC for $40 \leqslant T \leqslant 90$ K.

Table 2. Coefficients A_n, B_n, and C_n of the normalized in-plane resistivity ζ for stage-1 $Cu_cCo_{1-c}Cl_2$ GICs determined by a least-squares fit of the data to (15) in the temperature range between T_1 and T_2. T_0 is the characteristic temperature defined by $T_0 = B_n/C_n$.

c	A_n	B_n	C_n	T_0 (K)	T_1 (K)	T_2 (K)
0	0.428	6.599×10^{-4}	4.639×10^{-6}	142	20	290
0.20	0.540	2.118×10^{-4}	4.636×10^{-6}	45.7	20	290
0.30	0.787	5.951×10^{-4}	4.872×10^{-6}	1.22×10^{3}	20	290
0.70	0.518	1.584×10^{-3}	3.602×10^{-7}	4.40×10^{3}	20	290
1	0.067	3.252×10^{-3}	1.268×10^{-8}	2.56×10^{4}	80	300

[20, 21]. The resistivity ζ is proportional to T^2 for $T \gg T_0$ and proportional to T for $T \ll T_0$. The least-squares fit of these data to (15) yields the values of A_n, B_n, and C_n listed in table 2. From this table we find that T_0 drastically increases with increasing Cu concentration. This result indicates that as the Cu concentration increases, the exponent n of the power law for the resistivity gradually decreases from $n = 2$ to $n = 1$: $\zeta \approx T^n$. In fact the resistivity ζ is proportional to T^2 for $c = 0$ for $50 \leqslant T \leqslant 290$ K and is proportional to T for $c = 1$ for $80 \leqslant T \leqslant 290$ K.

Figure 9 shows the Cu concentration dependence of the non-magnetic contribution to

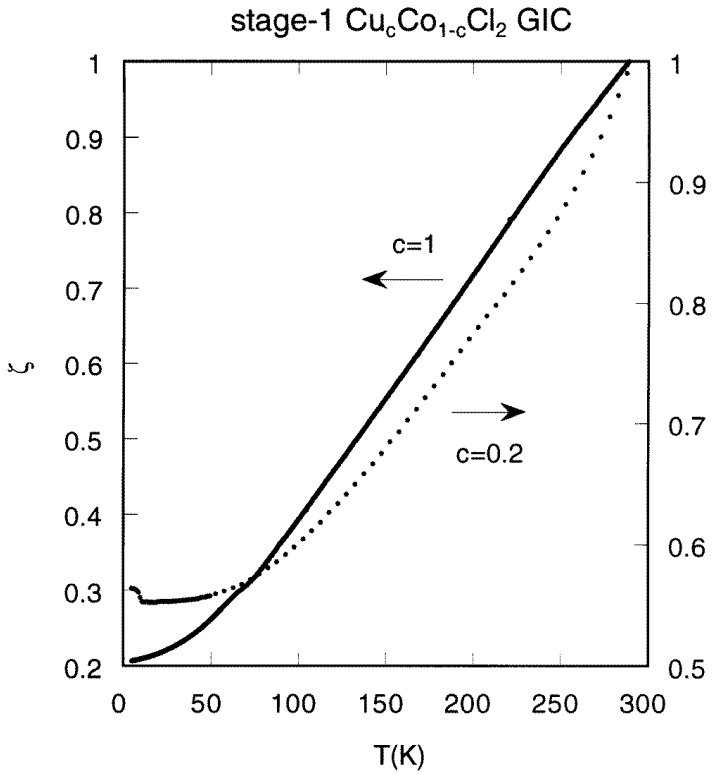

Figure 8. ζ versus T for stage-1 $Cu_cCo_{1-c}Cl_2$ GICs with $c = 0.20$ and $c = 1$ for the range $4.6 \leqslant T \leqslant 300$ K.

ζ at 5 K, λ, for stage-1 $Cu_cCo_{1-c}Cl_2$ GICs. The magnetic contribution to ζ is subtracted from λ for $c = 0$ and $c = 0.20$. Here we note that the value of λ is close to, but not exactly the same as that of the coefficient A_n. As shown in figure 9 the value of λ depends on the Cu concentration: it has a broad peak near $c = 0.5$ and minima at $c = 0$ and $c = 1$. These data seem to lie close to the solid line where λ varies with Cu concentration as $\lambda = (-0.238c + 0.447) + 1.452c(1 - c)$, which is the $c(1 - c)$-term plus the straight line between two end points at $c = 0$ and $c = 1$. For further discussion we assume that the in-plane resistivity at 290 K is independent of Cu concentration, in spite of lack of data on the absolute value of the resistivity for these compounds. Then the concentration dependence of λ is equivalent to that of the residual resistivity defined as the resistivity at 5 K. Since the electrical conduction of π-electrons occurs in the graphite layers, this residual resistivity is mainly due to the scattering of π-electrons by static lattice defects in graphite layers [22]. The residual resistivity due to the defect structures of the host graphite (ρ_r^1) is independent of the Cu concentration, while the residual resistivity due to the defect structures introduced during intercalation (ρ_r^2) depends on Cu concentration. The latter defect structures may be closely related to the degree of random distribution of Cu and Co atoms in the intercalate layers. For the degree of maximum randomness possible for a given value of c, the residual resistivity (ρ_r^2) is predicted to vary with the Cu concentration as $c(1-c)$ according to Nordheim's rule [23, 24]. As described above, in fact the variation of λ for stage-1 $Cu_cCo_{1-c}Cl_2$ GICs depends on the Cu concentration as $c(1-c)$. This result

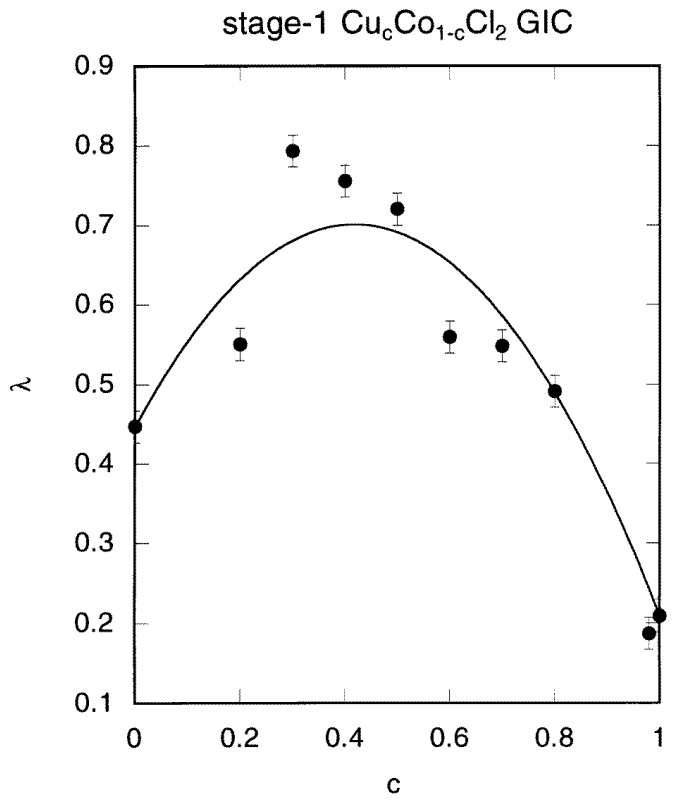

Figure 9. The non-magnetic contribution to ζ at 5 K, λ, versus the Cu concentration for stage-1 $Cu_cCo_{1-c}Cl_2$ GICs. The solid line is described by the equation $\lambda = (-0.238c + 0.447) + 1.452c(1-c)$.

gives indirect evidence that the Cu and Co atoms are randomly distributed on the triangular lattice in the intercalate layers.

4.4. The ac magnetic susceptibility

In order to determine the critical temperature T_c, the temperature dependence of the real part of the ac magnetic susceptibility (χ') for stage-1 $Cu_cCo_{1-c}Cl_2$ GICs with $c = 0.20$, 0.30, 0.40, and 0.50 has been measured for $4.6 \leqslant T \leqslant 25$ K. Figure 10(a) shows the plot of χ' versus T for stage-1 $Cu_cCo_{1-c}Cl_2$ GICs with $c = 0.30$ and $c = 0.40$. A broad peak is observed at around the critical temperature T_c: $T_c = 9.75 \pm 0.01$ K for $c = 0.30$ and 9.80 ± 0.01 K for $c = 0.40$. In figure 10(b) we show the plot of T_c versus Cu concentration c for stage-1 $Cu_cCo_{1-c}Cl_2$ GICs determined from the ac magnetic susceptibility and resistivity measurements. For comparison we also show the plot of T_c versus c for stage-2 $Cu_cCo_{1-c}Cl_2$ GICs determined from the ac magnetic susceptibility measurements [10]. The magnetic phase diagram of stage-1 compounds is essentially the same as that of stage-2 compounds in spite of the fact that the interplanar exchange interaction in stage-2 compounds is much weaker than that in stage-1 compounds. As shown in figure 10(b) the Cu concentration dependence of T_c for stage 1 agrees well with that for stage 2 for $0 \leqslant c \leqslant 0.40$. The increase

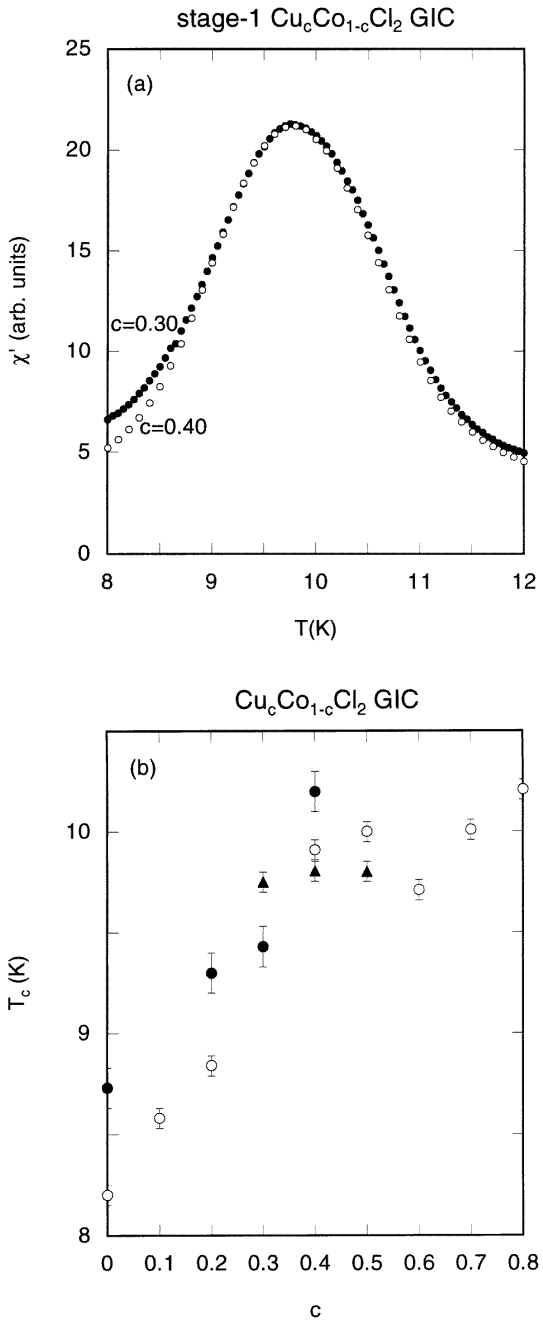

Figure 10. (a) The temperature dependence of the real part of the ac magnetic susceptibility (χ') for stage-1 $Cu_cCo_{1-c}Cl_2$ GICs with $c = 0.30$ (●) and 0.40 (○). (b) T_c versus the Cu concentration c for stage-1 $Cu_cCo_{1-c}Cl_2$ GICs determined from resistivity (●) and ac magnetic susceptibility measurements (▲). For comparison T_c versus the Cu concentration for stage-2 $Cu_cCo_{1-c}Cl_2$ GICs determined from ac susceptibility measurements (○) is also shown [10].

of T_c with increasing Cu concentration suggests that the intraplanar exchange interaction between Cu and Co, J(Cu–Co), is ferromagnetic rather than antiferromagnetic. In fact the Cu concentration dependence of the Curie–Weiss temperature Θ for stage-2 $Cu_cCo_{1-c}Cl_2$ GICs can be explained in terms of the ferromagnetic J(Cu–Co).

5. Discussion

5.1. Critical behaviour of magnetic resistivity

First we discuss the temperature dependence of the magnetic resistivity ζ_{mag} near T_c for stage-1 $Cu_cCo_{1-c}Cl_2$ GICs with $c = 0$, 0.20, 0.30, and 0.40. According to (5) and (7) in section 2, ζ_{mag} for stage-1 $Cu_cCo_{1-c}Cl_2$ GICs with $c \approx 0$ is expected to consist of the long-range spin-order part ζ_{LS} for $T < T_c$ and the spin-fluctuation part ζ_{LS} for both $T > T_c$ and $T < T_c$. Near T_c the in-plane resistivity of stage-1 $Cu_cCo_{1-c}Cl_2$ GICs is described by the sum of ζ_{mag} and the non-magnetic resistivity $\zeta_{non-mag}$. There are two methods for estimating $\zeta_{non-mag}$ near T_c: (i) the extrapolation of $\zeta_{non-mag}$ from the high-temperature side above T_c where $\zeta_{mag} \ll \zeta_{non-mag}$, and (ii) the suppression of $\zeta_{non-mag}$ near T_c by the application of an external magnetic field. Here we adopt the first method to determine the temperature dependence of ζ_{mag} near T_c. To this end we determine the polynomial function form of ζ versus T far above T_c where ζ is nearly equal to $\zeta_{non-mag}$, by the least-squares fitting of data to quadratic forms for $c = 0$ and $c = 0.20$ ($15 \leqslant T \leqslant 25$ K), a quadratic form for $c = 0.30$ ($16 \leqslant T \leqslant 35$ K), and a polynomial form to the fourth order for $c = 0.40$ ($12 \leqslant T \leqslant 25$ K). The dotted lines in figures 2–5 denote the extrapolation curves of $\zeta_{non-mag}$ versus T near T_c for $c = 0$, 0.20, 0.30, and 0.40. Note that the temperature dependence of ζ_{mag} for $c = 0.40$ is similar to that for $c = 0.50$ and 0.60 where ζ_{mag} is nearly equal to zero at any temperature. Figure 11(a) shows the temperature dependence of ζ_{mag} ($=\zeta - \zeta_{non-mag}$) for $c = 0$ and 0.20. The drastic increase of ζ_{mag} near T_c with decreasing temperature indicates that ζ_{LS} is predominant compared to ζ_{SF}. The long-range spin-order part ζ_{LS} is predicted to vary with temperature as $\zeta_{LS} \approx |t|^{2\beta}$ for $T < T_c$ from (7). Here we assume that the smearing of T_c due to either the macroscopic concentration gradient or inhomogeneity over the sample is described by a Gaussian distribution function with the average value $\langle T_c \rangle$ and width σ [25, 26]:

$$f(T_c) = \frac{1}{\sqrt{2\pi}\sigma} \exp\left[-\frac{1}{2}\left(\frac{T_c - \langle T_c \rangle}{\sigma}\right)^2\right]. \tag{16}$$

Then $\zeta_{LS}(T)$ can be rewritten as

$$\zeta_{LS}(T) = \int_T^\infty \zeta_0' \left(1 - \frac{T}{T_c}\right)^{2\beta} f(T_c)\ \mathrm{d}T_c \tag{17}$$

where ζ_0' is a constant. The least-squares fit of these data to (17) yields the values of β, $\langle T_c \rangle$, and σ: $\beta = 0.079 \pm 0.05$, $\langle T_c \rangle = 8.85$ K, and $\sigma = 0.62$ K for $c = 0$, and $\beta = 0.042 \pm 0.05$, $\langle T_c \rangle = 9.74$ K, and $\sigma = 1.22$ K for $c = 0.20$. These small values of β suggest that these compounds belong to a universality class of 2D XY spin systems. The value of $\langle T_c \rangle$ is in fairly good agreement with that of T_c for $c = 0$ and $c = 0.20$. The value of σ tends to increase with increasing Cu concentration, implying the increase of the concentration gradient or inhomogeneity over samples. These results indicate that ζ_{mag} is proportional to the square of the staggered magnetization $\langle \boldsymbol{S}(\boldsymbol{Q} = \boldsymbol{Q}_0) \rangle$. In stage-1 $CoCl_2$ GICs the 2D ferromagnetic layers are antiferromagnetically stacked along the c-axis for $T < T_c$. The magnetic neutron scattering intensity at $\boldsymbol{c}^*/2$ ($|\boldsymbol{c}^*| = 2\pi/d_1$) is proportional to

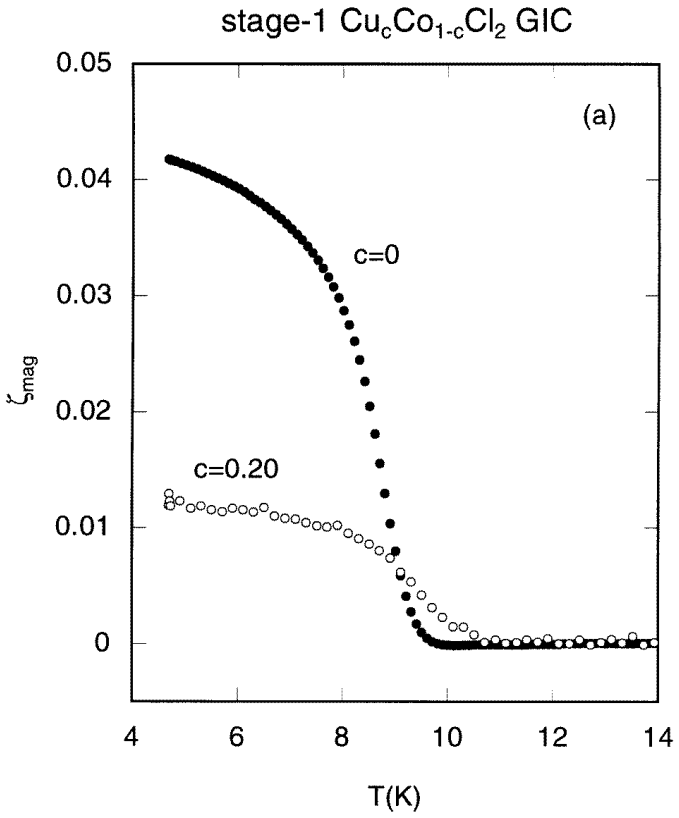

Figure 11. The magnetic resistivity ζ_{mag} versus T for stage-1 $Cu_cCo_{1-c}Cl_2$ GICs with (a) $c = 0$ (●) and 0.20 (○), and (b) $c = 0.30$ (●) and 0.40 (○), where $\zeta_{mag} = \zeta - \zeta_{non-mag}$. The solid line of the inset shows the fitting curve described by (18) with $\mu = 0.097$.

$|\langle \boldsymbol{S}(\boldsymbol{Q} = \boldsymbol{Q}_0)\rangle|^2$. In fact the integrated intensity at $\boldsymbol{c}^*/2$ is found to vary with temperature as $|t|^{2\beta}$ [27].

Our model described in section 2 predicts that the occurrence of ζ_{LS} below T_c is due to the scattering of π-electrons by antiferromagnetic in-plane spin configurations consisting of the superposition of the in-plane ferromagnetic spin structures of the N.N. magnetic intercalate layers separated by the graphite layer. The important conditions for the occurrence of ζ_{LS} below T_c in stage-1 $Cu_cCo_{1-c}Cl_2$ GICs are that (i) the effective antiferromagnetic interplanar exchange interaction J'_{eff} should be rather strong and that (ii) the antiferromagnetic spin alignment of the superimposed in-plane ferromagnetic spin structure should be described by a well-defined in-plane antiferromagnetic Bragg point at $\boldsymbol{Q} = \boldsymbol{Q}_0$. The latter condition also implies that the magnetic intercalate layers are structurally correlated along the c-axis.

Figure 11(b) shows the temperature dependence of ζ_{mag} for $c = 0.30$ and $c = 0.40$. For $c = 0.30$, ζ_{SF}, having a relatively sharp peak at around the peak temperature T_p ($=10.6 \pm 0.1$ K), is superimposed on ζ_{LS}, which tends to reduce to zero at around T_p with increasing temperature. The slight deviation of T_p from T_c ($=9.75 \pm 0.01$ K) determined from the ac magnetic susceptibility χ' is partly due to the superposition of ζ_{LS} and ζ_{SF} near T_p. For $c = 0.40$, ζ_{LS} almost disappears, while ζ_{SF} still has a relatively sharp peak at around T_p

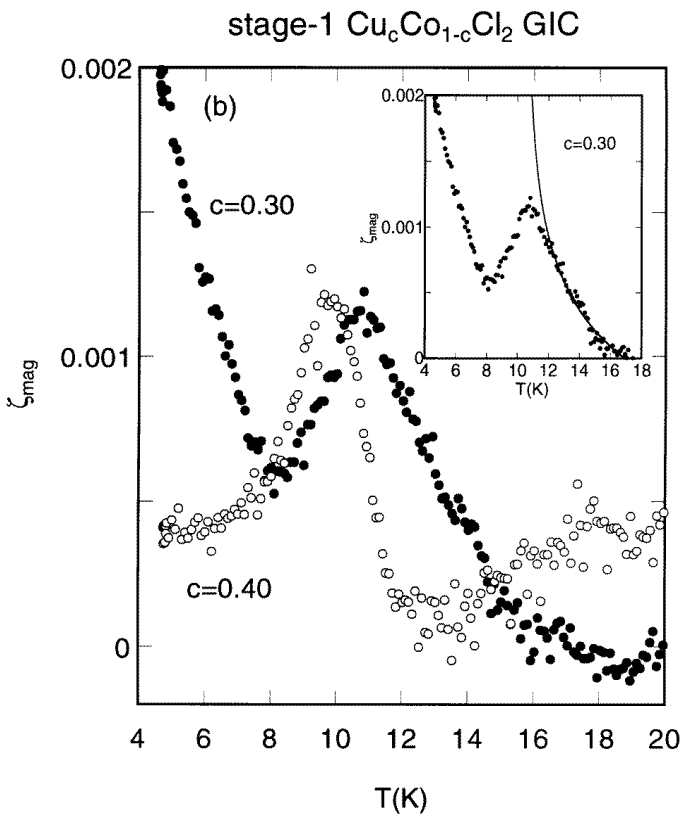

Figure 11. (Continued)

(=9.9±0.1 K) close to T_c (=9.80±0.01 K) determined from the ac magnetic susceptibility. The disappearance of long-range spin order with increasing Cu concentration is due to the spin-frustration effect arising from competing ferromagnetic and antiferromagnetic intraplanar exchange interactions. This tendency of the disappearance of ζ_{LS} is consistent with the results derived from the value of the dc magnetic susceptibility at 5 K versus the Cu concentration for stage-2 $Cu_cCo_{1-c}Cl_2$ GICs [10]. Note that no appreciable spin-fluctuation part is observed for stage-1 $Cu_cCo_{1-c}Cl_2$ GICs with $0.50 \leqslant c \leqslant 0.90$ in spite of the fact that ferromagnetic phase transitions still weakly occur near 10 K. The degree of spin ordering in these compounds is strongly influenced by the competing intraplanar exchange interactions J(Co–Co), J(Cu–Co), and J(Cu–Cu). The interaction J(Cu–Co) also varies with the Cu concentration. For $0 \leqslant c \leqslant 0.20$ there exists a ferromagnetic long-range order of Co^{2+} spins in the intercalate layers. For $c > 0.50$ the ferromagnetic interaction J(Cu–Co) contributes to the ferromagnetic long-range order, while the antiferromagnetic interaction J(Cu–Cu) tends to suppress this order. The interaction J(Cu–Co) is of the same order as J(Co–Co) at $c = 0.50$, increases with increasing Cu concentration, and becomes of the same order as $|J(\text{Cu–Cu})|$ at $c \approx 0.80$.

Next we discuss the critical behaviour of ζ_{SF} for $c = 0.30$. The spin-fluctuation part ζ_{SF} is predicted to vary with temperature as $\zeta_{SF} \approx |t|^{\nu(-1+\eta)}$ for $T > T_c$ and $|t|^{\nu'(-1+\eta')}$ for

$T < T_c$ from (5) and (7). For convenience we assume that ζ_{SF} is described by

$$\zeta_{SF}(t) = \frac{A}{\mu}(t^{-\mu} - 1) + B \tag{18}$$

where $t = T/T_c - 1$, A and B are constant or only weakly temperature dependent, and μ is the exponent which characterizes the resistive critical behaviour. When $\mu = 0$, the divergence is logarithmic. The least-squares fit of the data on ζ_{SF} versus T for $0.13 \leqslant t \leqslant 0.70$ to (18) yields $\mu = 0.097 \pm 0.123$ and $A = (-2.90 \pm 0.40) \times 10^{-4}$. The fitting curve thus obtained is denoted by a solid line in the inset of figure 11(b). In this analysis we use T_p (=10.6 K) instead of T_c (=9.75 K), although small errors in T_c may significantly affect the critical region results. Such an assumption precludes a precise statement about the critical exponent μ: the data are consistent with $\mu \approx 0.1$. This value of μ is much smaller than that predicted from (5) and (7): $\mu = \nu(1 - \eta) \approx 1$, since $\eta \approx 0$ and $\nu \approx 1$ for stage 1 $Cu_cCo_{1-c}Cl_2$ GICs which magnetically behave like 2D XY spin systems. Before further discussion we note that similar analysis for ζ_{SF} versus T with $c = 0.40$ was unsuccessful partly because the critical exponent μ thus obtained strongly depends on the background term including $\zeta_{non-mag}$. What is the reason for such a large difference of μ? As described in section 2, the spins separated by a distance greater than the electron mean free path cannot scatter π-electrons coherently [15]. When the in-plane spin-correlation length is larger than the mean free path, the spin fluctuations do not contribute to ζ_{mag}. The mean free path remains finite through T_c and is typically hundreds of Å [2]. The spin-fluctuation part of ζ_{mag} is determined by the Fourier transform of the in-plane spin-correlation function, $\Gamma(\boldsymbol{k})$ with $\boldsymbol{k} = \boldsymbol{Q} - \boldsymbol{Q}_0$. The long-range part of $\Gamma(\boldsymbol{k})$, where the in-plane spin-correlation length is larger than mean free path, does not contribute to ζ_{SF}. Therefore it is not reasonable to suppose that the detailed form of ζ_{SF} is determined solely by the long-range part of $\Gamma(\boldsymbol{k})$ with $k \approx 0$.

5.2. Superexchange interaction and $\pi-d$ exchange interaction

We consider the $\pi-$d exchange interaction $J_{\pi-M}$ (M = Co and Cu) which is responsible for ζ_{mag} in stage-1 $Cu_cCo_{1-c}Cl_2$ GICs. In these compounds the intraplanar exchange interaction is dominated by the superexchange mechanism [28–30]. The superexchange interaction between M^{2+} ions occurs through the Cl^- ions ($(3p)^6$), where one of two bonds denoted by M–Cl is perpendicular to the other bond denoted by M′–Cl (the $\phi = 90^\circ$ case). Because of the overlap of electron wave functions, one of the 3p electrons from the Cl^- ion hops over to the M^{2+} ion. The remaining unpaired 3p electron on the Cl^- ion then enters into a direct exchange with the M'^{2+} ion with an exchange interaction $J_{M'-Cl}$. The intraplanar exchange interaction between M and M′ ions can be described by $J_{M-M'} = \varepsilon^2 J_{M'-Cl}/S^2$, where S is the spin of M^{2+}, $\varepsilon = b/U$, and b, U, and ε^2 are the energy matrix element, the increase of energy, and the probability for shifting the 3p electron to M^{2+}, respectively. The energy level of a 3d electron in the octahedral crystal field splits into the dε and dγ levels: the dε level lies lower than the dγ level. The ground state of M^{2+} in the MCl_2 GIC is an orbital doublet for Cu^{2+} and an orbital triplet for Co^{2+}. The single one-electronic configuration of the lowest orbital state of M^{2+} is $(d\varepsilon^6)(d\gamma^2)d\gamma^1$ for Cu^{2+} and $\approx(d\varepsilon^4)d\varepsilon^1 d\gamma^2$ for Co^{2+} [28] (the parentheses indicate paired electrons). The p orbitals of the 3p electrons are denoted by p_σ and p_π, where the p_σ orbital is the p orbital whose principal axis points to M^{2+} ion, and the p_π orbital is the p orbital whose principal axis is perpendicular to the line connecting the Cl^- ion.

According to the method used by Sugihara *et al* [2], the $\pi-$d exchange Hamiltonian is described by $H_{\pi-M} = -2J_{\pi-M}(\boldsymbol{\sigma} \cdot \boldsymbol{S})$, where $J_{\pi-M} = \alpha\varepsilon^2 J_{\pi-Cl}$ with $\alpha = 1.35$ for

Co^{2+} and $\alpha = 3$ for Cu^{2+}, and $J_{\pi-Cl}$ is the exchange interaction between the spin of the π-electron and the unpaired 3p electron of Cl^-. Then the $\pi-$d exchange interaction $J_{\pi-M}$ can be rewritten as

$$J_{\pi-M} = \frac{\alpha}{S^2}\frac{J_{M-M'}}{J_{M'-Cl}}J_{\pi-Cl} \tag{19}$$

in terms of $J_{M-M'}$, where $S = 1/2$ for both the Cu^{2+} spin and the fictitious spin of Co^{2+}. The intraplanar exchange interaction $J_{M-M'}$ is experimentally determined as 7.75 K for the $CoCl_2$ GIC and -39 K for the $CuCl_2$ GIC, which implies that $J_{Co'-Cl} > 0$ and $J_{Cu'-Cl} < 0$. It may be reasonable to assume that $J_{\pi-Cl}$ of the $CoCl_2$ GIC is equal to that of the $CuCl_2$ GIC because the graphite layer is sandwiched between two Cl^- layers. Then the ratio of $J_{\pi-Co}$ to $J_{\pi-Cu}$ is expressed by

$$\frac{J_{\pi-Co}}{J_{\pi-Cu}} \approx -0.1\frac{J_{Cu'-Cl}}{J_{Co'-Cl}}. \tag{20}$$

Since one M–Cl bond is perpendicular to the other M′–Cl bond, the p_σ and p_π orbitals for the M–Cl bond are the p_π and p_σ orbitals, respectively, for the M′–Cl bond. The d orbitals of the M'^{2+} ion are denoted as $d\varepsilon'$ and $d\gamma'$ orbitals. A set of empirical rules (the Goodenough–Kanamori rules [28, 30]) are well established for determining the sign of $J_{M'-Cl}$ or $J_{M-M'}$ from the symmetry relation between the occupied d orbitals ($d\varepsilon$ and $d\gamma$) and occupied p orbitals (p_σ and p_π). For the $CoCl_2$ GIC the p_π orbital of the Cl^- ion is non-orthogonal to the $d\varepsilon$ orbital of one Co^{2+} ion and orthogonal to the $d\varepsilon'$ orbital of the other Co'^{2+} ion. Less than one electron transfers from the p_π orbital to the $d\varepsilon$ orbital. The electron left behind on the Cl^- ion has its spin parallel to the spin of the Co^{2+} ion. The direct exchange interaction between the p_π orbital and $d\varepsilon'$ orbital of the Co'^{2+} ion, $J_{Co'-Cl}$, is ferromagnetic because of the orthogonality [28]. Therefore the intraplanar exchange interaction between Co^{2+} spins is ferromagnetic, which is consistent with the experimental result: $J_{Co-Co'} = 7.75$ K. For the $CuCl_2$ GIC the p_σ orbital is non-orthogonal to the $d\gamma$ orbital of the Cu^{2+} ion and orthogonal to the $d\gamma'$ orbital of the Cu'^{2+} ion. Less than one electron transfers from the p_σ orbital to the $d\gamma$ orbital. This $d\gamma-p_\sigma$ bond is stronger than the $d\varepsilon-p_\pi$ bond for the $CoCl_2$ GIC because of a larger overlap of wave functions. The electron left behind on the Cl^- ion has its spin parallel to the spin of the Cu^{2+} ion. The direct exchange interaction between the p_σ orbital and the $d\gamma'$ orbital of the Cu'^{2+} ion is ferromagnetic because of the orthogonality [28]. Thus the intraplanar exchange interaction between Cu^{2+} spins is ferromagnetic, which is inconsistent with the experimental result: $J_{Cu-Cu'} = -39$ K. Since the Cu^{2+} ion is a Jahn–Teller ion and the ground state is an orbital doublet, the ground state may be no longer described by the single one-electron configuration of $(d\varepsilon^6)(d\gamma^2)d\gamma^1$ [28]. These situations may favour the antiferromagnetic interaction rather than the ferromagnetic one. In spite of this the direct exchange interaction $J_{Cu'-Cl}$ may dominantly include the element of the $p_\sigma-d\gamma'$ coupling.

At the present we do not know how to estimate the magnitude of the direct exchange interactions $J_{Co'-Cl}$ and $J_{Cu'-Cl}$. Experimentally no appreciable magnetic resistivity is observed for $0.50 \leqslant c \leqslant 0.90$, suggesting that the magnitude of $J_{\pi-Cu}$ is smaller than that of $J_{\pi-Co}$. This may imply that the magnitude of $J_{Cu'-Cl}$ is larger than that of $J_{Co'-Cl}$.

6. Conclusion

We have studied the temperature dependence of the in-plane magnetic resistivity for stage-1 $Cu_cCo_{1-c}Cl_2$ GICs. The magnetic resistivity near T_c consists of a long-range spin-order

part and a spin-fluctuation part. The long-range spin-order part observed for $0 \leqslant c \leqslant 0.30$ is proportional to the square of the staggered magnetization with a smeared power law with exponent 2β. The spin-fluctuation part observed for $c = 0.30$ seems to diverge with an exponent μ ($\approx$0.1) which is much smaller than the expected exponent $\nu(1-\eta)$ as the temperature approaches T_c from the high-temperature side: $\nu(1-\eta) \approx 1$ for 2D XY ferromagnetic systems. This implies that the long-range part of the spin fluctuations cannot contribute to the magnetic resistivity since the in-plane spin-correlation length is larger than the mean free path. Both parts disappear for $c \geqslant 0.50$ in spite of the existence of a ferromagnetic phase transition for $c < 0.90$. For $c = 1$ there exists a resistive anomaly related to the growth of short-range spin order which is a characteristic of the 2D Heisenberg antiferromagnet. These behaviours can be qualitatively explained in terms of a model in which through $\pi-$d exchange interactions the π-electrons are scattered by the spins of the antiferromagnetic in-plane spin configuration arising from the superposition of two ferromagnetic in-plane spin structures.

Further study on the $\pi-$d exchange interaction ($\pi-Co^{2+}$ and $\pi-Cu^{2+}$) is required for understanding the conduction mechanism of π-electrons in stage-1 $Cu_cCo_{1-c}Cl_2$ GICs.

Acknowledgments

We would like to thank H Suematsu and Y Hishiyama for providing us with single-crystal kish graphite, and A Moore for providing us with HOPG. We would like to thank J Morillo, M D Johnson, and A Tafti for their help with sample preparation and x-ray scattering measurements. We are grateful to C R Burr for a critical reading of this manuscript. This work was supported by NSF DMR 9201656.

References

[1] Yeh N-C, Sugihara K, Dresselhaus M S and Dresselhaus G 1989 *Phys. Rev.* B **40** 622–35
[2] Sugihara K, Yeh N-C, Dresselhaus M S and Dresselhaus G 1989 *Phys. Rev.* B **39** 4577–87
[3] Kinany-Alaoui M, Piraux L, Bayot V, Issi J P, Pernot P, and Vangelisti R 1989 *Synth. Met.* **34** 537–42
[4] Pernot P and Vangelisti R 1989 *Z. Naturf.* b **44** 761–6
[5] McRae E, Herold A, LeLaurain M, Mareche J F, Perignon A, Pernot P and Vangelisti R 1988 *Symp. on Graphite Intercalation Compounds at the Materials Research Society Meeting* ed M Endo, M S Dresselhaus and G Dresselhaus (Pittsburgh, PA: Materials Research Society Press) extended abstracts, pp 105–8
[6] Piraux L 1994 *Mol. Cryst. Liq. Cryst.* **245** 67–74
[7] Nicholls J T and Dresselhaus G 1990 *J. Phys.: Condens. Matter* **2** 8391–404
[8] Nicholls J T and Dresselhaus G 1990 *Phys. Rev.* B **41** 9744–51
[9] Suzuki M, Suzuki I S, Olson B and Shima T 1996 *J. Phys.: Condens. Matter* **8** 199–216
[10] Suzuki M, Suzuki I S, Johnson M, Morillo J and Burr C R 1994 *Phys. Rev.* B **50** 205–15
[11] Suzuki M, Suzuki I S, Burr C R, Wiesler D G, Rosov N and Koga K 1994 *Phys. Rev.* B **50** 9188–99
[12] Dresselhaus G, Nicholls J T and Dresselhaus M S 1992 *Graphite Intercalation Compounds II* ed H Zabel and S A Solin (Berlin: Springer) pp 247–345
[13] Suzuki M 1990 *Crit. Rev. Solid State Mater. Sci.* **16** 237–54
[14] de Gennes P G and Friedel J 1958 *J. Phys. Chem. Solids* **4** 71–7
[15] Fisher M E and Langer J S 1968 *Phys. Rev. Lett.* **20** 665–8
[16] Wiesler D G, Suzuki M, Chow P C and Zabel H 1986 *Phys. Rev.* B **34** 7951–7
[17] Hendricks S and Teller E 1942 *J. Chem. Phys.* **10** 147–67
[18] Suzuki I S and Suzuki M 1994 *J. Phys.: Condens. Matter* **3** 8825–30
[19] Navarro R 1990 *Magnetic Properties of Layered Transition Metal Compounds* ed L J de Jongh (Boston, MA: Kluwer–Academic) pp 105–90 (see also its references)
[20] Kamimura H, Nakao K, Ohno T and Inoshita T 1980 *Physica* **99** B&C 401–5
[21] Inoshita T and Kamimura H 1981 *Synth. Met.* **3** 223–7
[22] Issi J P 1992 *Graphite Intercalation Compounds II* ed H Zabel and S A Solin (Berlin: Springer) pp 195–245

[23] Nordheim L 1931 *Ann. Phys., Lpz.* **9** 641
[24] Mott N F and Jones H 1958 *The Theory of the Properties of Metals and Alloys* (New York: Dover) pp 297–302
[25] Birgeneau R J, Als-Nielsen J and Shirane G 1977 *Phys. Rev.* B **16** 280–92
[26] Ikeda H, Suzuki M and Hutchings M T 1979 *J. Phys. Soc. Japan* **46** 1153–60
[27] Ikeda H, Endoh Y and Mitsuda S 1985 *J. Phys. Soc. Japan* **54** 3232–5
[28] Kanamori J 1959 *J. Phys. Chem. Solids* **10** 87–98
[29] Anderson P W 1963 *Solid State Physics* vol 14, ed F Seitz and D Turnbull (New York: Academic) pp 99–214
[30] Goodenough J B 1963 *Magnetism and the Chemical Bond* (New York: Wiley)